The Magellan Telescopes: A Performance Update

The Magellan Telescopes: A Performance Update

Povilas Palunas[1a], David Floyd[b,c], Glenn Eychaner[a], David J. Osip[a], Paul Schechter[d]
[a]Observatories of the Carnegie Institution, 813 Santa Barbara St, Pasadena, CA 91101
[b]Anglo-Australian Observatory, PO Box 296, Epping, NSW 2121, Australia
[c]School of Physics, University of Melbourne, VIC 3010, Australia
[d]MIT, 77 Massachusetts Avenue, 37-664G, Cambridge, MA 02139

ABSTRACT

The Magellan Baade and Clay telescopes regularly produce images of ~0.5" in natural seeing. We review efforts to improve collimation, active optics response, and telescope guiding and pointing to optimize the performance of the telescopes. Procedures have been developed to monitor and analyze image quality delivered by the imaging science instruments. Improved models have been developed to correct for flexure of the telescope and primary mirror under gravity loading. Collimation has been improved using a "two-probe" Shack-Hartman technique to measure field aberrations. Field acquisition performance has been improved by implementing an open loop model for the primary mirror control. Telescope pointing has been improved by regular monitoring and adjustments to improve acquisition times.
Keywords: telescopes, active optics, mirror support

1. INTRODUCTION

The Magellan 6.5-meter telescopes at the Las Campanas Observatory were commissioned nearly a decade ago. The Baade telescope has been in science operations since February, 2001 and the Clay telescope since September 2002. The optical design is presented by Shectman[1]. The as-built telescopes and early operations are described by Shectman[2] and Shectman & Johns[3] respectively. The observatory is currently in the process of commissioning a set of second generation instruments including: MegaCam (a 1/2 degree imager), MMIRS (a multi-object NIR spectrograph), PFS (the planet finder spectrograph), FIRE (a NIR echellette spectrograph), FourStar(a wide field NIR imager). MegaCam and MMIRS are fed by a new f/5 Cassegrain secondary. In addition, an adaptive optics secondary is in construction and expected to be installed in 2012.

In this paper we show the current imaging performance of the Magellan telescopes and describe various activities to optimize the telescope operations.

2. MAGELLAN ACTIVE OPTICS

The first generation of the Magellan facility guiders are described by in detail by Schechter[3]. The systems consist of two identical probes, each of which can be positioned to cover a rectangular field of 7.7' by 12.9' on its side of the guider. Each probe also has a focus stage which is used to follow the focal surface curvature of the telescope. Each probe has a selectable stage which allows it to be used as either a guider or a Shack-Hartmann (S-H) wavefront sensor. In normal operations one probe is used for off-axis guiding and the other for off-axis wavefront sensing. The guide star images are analyzed to give a real time estimate of the image quality of the telescope, however, the guider optics are not capable of producing images better than about 0.4 " (FWHM).

The active optics system corrects figure errors in the primary mirror (M1) and the on-axis alignment errors of the secondary mirror (M2). The tilt measurement of the wavefront sensor is used as a reference to correct for field rotation errors. In addition to compensating for focal surface curvature by changing the focus of the S-H probe the wavefront measurements are compensated for astigmatism and coma field aberrations in order to achieve the best imaging on-axis. Coma corrections are made by tilting the secondary mirror about a point defined by its center of curvature, which

[1] palunas@lco.cl; phone +5651203612

Ground-based and Airborne Telescopes III, edited by Larry M. Stepp, Roberto Gilmozzi, Helen J. Hall
Proc. of SPIE Vol. 7733, 77331I · © 2010 SPIE · CCC code: 0277-786X/10/$18 · doi: 10.1117/12.857805

maintains constant pointing for the telescope. The astigmatism and coma corrections are calculated under the assumption of a well collimated telescope. Procedures for collimating the telescope are discussed below.

Figure 1 shows an image of a facility guider. The facility guiders are currently in version 3 which includes modifications to make them more robust and simplify setup. The primary changes in version 3 are: (1) An optional coarse lenslet array in wavefront sensor was eliminated, (2) The stage lead screws were replaced with ones with finer threads to improve non-sidereal guiding and (3) Most adjustable stops have been replaced with precision machined hard stops.

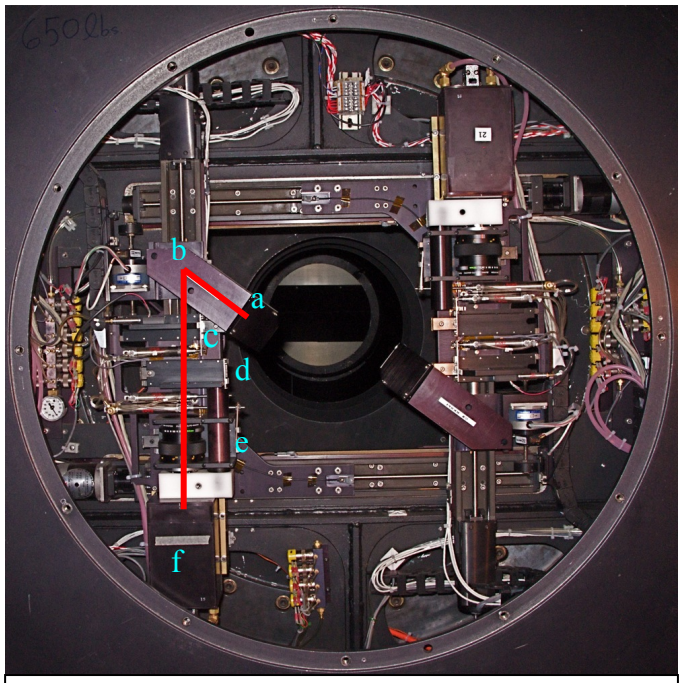

Figure 1 Magellan guider. There are two identical probes on the left and right. The red line shows the optical path...a and b indicate fold mirrors. c selects between a field lens an for imaging and an aperture for wavefront sensing. An additionional stage inserts an LED illuminated pinhole for creating S-H templates. d is a filter slide with a red filter and a clear aperature.. e selects between a re-imaging lens and S-H collimator and lenslet assembly. f is the CCD detector.

2.1 Wavefront Basis Functions

The wavefront is analyzed with a blend of Zernike and mirror bending modes. The Zernike focus and coma modes are used to control the position of the secondary mirror and a subset of the bending modes are used to control the primary mirror figure. The mirror bending modes are derived by a Singular Value Decomposition (SVD) of the influence function of the primary mirror force actuators on the primary mirror surface figure[5][6][7]. To keep the mind sharp, the bending modes and Zernikes are stored in tables as standard Zernikes (rms normalized) defining the surface, while for wavefront analysis they are converted to standard Zernikes defining the wavefront (2× surface) and offsets and field corrections are made in terms of fringe Zernikes (edge normalized) defining the wavefront.

Using mirror bending modes has the advantage allowing control of the primary mirror figure using substantially less force than required with a pure Zernike mode analysis. In practice, the use of bending modes reduces the required force on the primary by a factor of 1.5 and improves the delivered FWHM of the telescope by a similar factor. Most of the bending modes are easily recognizable as standard aberrations such as astigmatism, coma and trefoil. Although these bending modes are quite similar to the corresponding Zernikes they are not the same. A principal difference between the bending modes and Zernikes is that the bending modes break the requirement of Zernikes that the functions be both even or both odd in radius and azimuth . The lowest order such bending mode has a linear radial component (which is odd radially) and is circularly symmetric (which is even azimuthally). The functional form of the mode prompts the name: cone mode. Expanded in terms of Zernike polynomials the cone mode includes terms for all of the circularly symmetric Zernike modes. Cone mode is driven primarily through temperature irregularities across the primary mirror and can, very occasionally, become large enough to exceed the force limits needed to control it when the primary mirror is poorly conditioned.

The disadvantage of using the bending modes is that they do not contain the modes needed to control the secondary mirror. There is no mode that corresponds to Zernike focus, and the bending coma modes are not the same as the Zernike coma modes. The Zernike focus mode is therefore added to the bending modes, and the bending modes that correspond to coma are substituted by the corresponding Zernike modes. A problem with this configuration is that the focus and cone modes are partially degenerate. This can lead to instabilities in the control system which in turn leads to either longer settling times or possibly a growing instability. With the facility guiders such instabilities have not been a significant issue. There have, however, been issues with the wavefront sensors on MMIRS which have approximately 30% coarser sampling than the facility guiders and are therefore more sensitive to the degeneracies between the modes.

To demonstrate the problem of mixing the Zernike and bending modes we reverse our method and decompose the mirror bending modes in terms of the first 15 standard Zernikes with the addition of a "cone mode" which has the form 3*r*-2. The choice of function is piston free and normalized to both fringe and standard Zernikes but is not orthogonal to all the Zernikes. Table 1 shows the amplitudes of the Zernike modes in the decomposition of the bending modes. The rms residuals to the decomposition are given at the bottom of the table.

Table 1. Decomposition of Magellan primary mirror bending modes B_i into Zernikes plus a (3r-2) cone mode

	B_0	B_1	B_2	B_3	B_4	B_5	B_6	B_7	B_8	B_9	B_{10}	B_{13}
Z_1 piston	0.02	0	0.11	0	0	0	0	0	0	0.03	0	0.12
Z_2 tilt-c	-0.01	-0.01	0.01	-0.01	0	0	0.08	0	0	0	0	-0.01
Z_3 tilt-s	0.01	-0.01	0.01	0	-0.02	0.08	0	0	0	-0.01	0	-0.01
Z_6 astig-c	0.95	0	-0.09	0.01	0.01	-0.01	0.01	0.01	0	0.05	0	0
Z_5 astig-s	0	0.95	0	-0.01	0.01	0.01	0	0	0.04	0	-0.05	0
3*r*-2 cone	-0.06	0	-1.05	0	-0.02	0.04	0.05	0.12	0	-2.24	0	-14.6
Z_4 focus	-0.05	0	-0.27	0	0.01	-0.02	-0.03	-0.08	0	1.49	0	9.86
Z_{10} tref-c	0	0	0	-0.93	0	0	-0.08	-0.01	-0.01	0.01	0.01	0
Z_9 tref-s	0	0	0	0	-0.93	-0.08	0	0.01	-0.01	0.01	-0.01	0
Z_7 coma-s	0	0	0	0	0.08	-0.86	0	0	0	-0.01	-0.01	-0.01
Z_8 coma-c	0	0	0	0.07	0	0	-0.86	0	0	0	-0.01	-0.01
Z_{14} quad-c	0	0	0	0	0	0	0	0.91	0	-0.02	0	0.02
Z_{15} quad-s	0	-0.02	0	0	0	0	0	0	0.91	0	0.14	0
Z_{12} astig5-c	-0.06	0	0.02	0	0	0	0	-0.03	0	-0.83	0	0.14
Z_{13} astig5-s	0	-0.05	0	0	0	0	0	0	-0.14	0	0.84	0
Z_{11} spherical	0.01	0	0.06	0	0	0	0	0	0	-0.06	0	-0.69
rms	0.01	0.01	0.01	0.11	0.10	0.30	0.30	0.17	0.16	0.43	0.45	0.16

The ordering of the Zernike plus cone modes in the table has been arranged to correspond to the order of the mirror bending modes, which are in order of increasing stiffness. The shaded diagonal of the table shows that most of the bending modes correspond reasonably well to Zernike modes having coefficients close to unity. The bending cone mode, B_2, is primarily a mixture of 3*r*-2 cone mode and Zernike focus. The bending modes that correspond to coma, B_5 and B_6, have significant contributions from other modes. The modes B_9 and B_{13} have large amplitudes with opposite signs for cone and focus modes, demonstrating the danger of instability when using degenerate modes. In addition to the control problems with the MMIRS wavefront sensor this effect likely contributes to lower level instabilities in the cone mode discussed in the primary mirror section below.

An alternative way of separating the secondary positioning from the primary mirror aberrations is to fit the wavefront sensor data to a set purely orthonormal modes, such as the bending modes, and project out the Zernike focus and coma modes. Equation 1 provides an example for Zernike focus

$$\begin{aligned} \vec{E}(x,y) &= \sum_i d_i B_i(x,y) \\ \vec{Z}_4(x,y) &= \sum_i c_i B_i(x,y) \\ k_f &= \vec{Z}_4 \cdot \vec{E} \\ \vec{E}_{\mathrm{M1}} &= \vec{E} - k_f \vec{Z}_4 \end{aligned} \quad . \tag{1}$$

where $\vec{E}$ is the wavefront error, B_i are the bending modes d_i are the coefficients of the wavefront expansion, $\vec{Z}_4$ is Zernike focus expanded in terms of bending modes with coefficients c_i, k_f is the contribution of Zernike focus to the to the wavefront error and $\vec{E}_{\mathrm{M1}}$ is the residual wavefront error in the primary mirror. A similar procedure can be carried out for Zernike coma to compensate for secondary alignment. This method eliminates issues with fitting degenerate functions. In this method care must be taken to include in the fit to the wavefront error all modes that significantly contribute to the Zernike focus and coma expansions.

3. ON-AXIS COLLIMATION

The telescope is normally collimated when a secondary mirror is installed or after major primary mirror maintenance. Initial collimation is performed using a K&E autocollimating telescope. The collimation is checked at various elevations and a flexure model is constructed. The procedure has been found to be very consistent but also to yield substantial residual errors in the optical wavefront. After the mechanical alignment with the autocollimator telescope the collimation and flexure models are improved using the S-H wavefront sensor. The active optics control is run on-axis to convergence at a range of different elevations for the telescope. The corrected secondary mirror positions are recorded at each elevation and a refined flexure model is constructed for the telescope.

4. FULL COLLIMATION

A classical Gregorian or Cassegrain telescope exhibits circularly symmetric focus, astigmatism and focal surface field aberrations which become significant over wide fields[8][9]. The focus and astigmatism field aberrations increase quadratically with field angle while the coma increases linearly. The focus field aberration is referred to as field curvature. In a well collimated telescope these aberrations patterns are co-aligned and centered at the nominal axis of the telescope. On the Magellan telescopes the nominal axis is defined as going through the rotation center of the instrument rotators. Mis-collimation of the primary, secondary and a possible tertiary mirror shifts these aberration patterns with respect to the nominal axis and with respect to each other.

A lateral translation of the secondary shifts the coma pattern. The focus pattern remains unchanged and the astigmatism pattern changes by only a very small, insignificant amount.

A tilt of the secondary about its vertex shifts all three of the patterns and tilts the focus pattern. The focal surface curvature is very nearly spherical, \ and for a spherical surface tilt and shift transformations are degenerate. Because of this, the focal pattern tilt can be considered the same as an additional focal pattern shift. When the secondary is tilted the focus and coma patterns shift in one direction and the astigmatism pattern shifts in the opposite direction. It is possible to translate and tilt the secondary so that the coma pattern does not move. The combined translation and tilt of the secondary about its vertex can be considered as a pure tilt around a point on the optical axis of the primary. This point is called the coma neutral point and for paraxial rays is coincident with prime focus. On the Magellan telescopes for the f/11 secondary this point is 1594mm below the secondary vertex. Rotations about the coma neutral point change the pointing of the telescope and the coma pattern follows the pointing. By offsetting the rotation point from the prime focus it is possible to keep the coma unchanged on the instrument axis. On the Magellan telescopes this point is 19 mm from prime focus toward the primary. On the Magellan telescopes the secondary support and positioning structure is designed so that tilts are introduced at a point close to the coma neutral point. Small tilts around the coma neutral point produce little astigmatism on-axis because of the quadratic field dependence.

For a Nasmyth or folded port a tilt of the tertiary mirror shifts all three patterns in the same direction with respect to the nominal axis. If there are no additional optics between the tertiary and the focal surface, calculating the shift is a simple geometric problem. For astigmatism and coma the shift is $2\theta d$ for rotations about an axis perpendicular to the fold, where θ is the angle of the tilt and d is the distance to the focal plane (5004mm for Magellan without the ADC). The focus pattern shifts somewhat more because of the focal plane tilt as discussed above (~30% more for Magellan). Note that rotations about an axis in the plane of the fold are $\sqrt{2}$ smaller for a 90° fold. Once again, by combining a tilt of the tertiary with lateral translation of the secondary it is possible to leave the coma pattern stationary.

4.1 Two-Probe Collimation

For narrow field instruments it is still critical to have a well collimated telescope in order to successfully perform off-axis wavefront sensing. We use a technique to measure the field aberrations using both probes of the guider as wavefront sensors. One probe is set at center field and is used actively. The second probe is used passively to measure the wavefront at different field positions. A similar technique has been used by Gitton[10]. The active control is setup to null coma at the centerfield by moving the secondary only in translation, this prevents the focus and astigmatism patterns from moving during the test. The cone mode correction is also turned off to prevent any change in the focus measure caused by degeneracies between cone mode and focus. The data acquisition is set up so that the wavefronts at the active probe and at the passive probe are acquired simultaneously, this allows small errors in the active control to be subtracted from the passive measurement. The passive probe is used to measure only the following Zernike terms: focus,

astigmatism, coma and spherical. Thus far, the center probe has been used to measure and correct mixed bending and Zernike modes (excluding cone mode).

In the two-probe measurements the field aberrations are measured with respect to those expected for a well collimated telescope with the wavefront sensor focus placed on the nominal focal surface. The differential nature of these measurements reduces the functional dependence of the aberration errors by one order over that of the functional form of the aberration patterns. The error in the focus (Z_3) and astigmatism (Z_4, Z_5) are, therefore, linear across the field and the error in the coma (Z_6, Z_7) is a constant over the field.

$$\begin{aligned} \Delta Z_3 &= -2C_f(xx_f - yy_f) \\ \begin{pmatrix} \Delta Z_4(x,y) \\ \Delta Z_5(x,y) \end{pmatrix} &= -2C_a \begin{pmatrix} xx_a - yy_a \\ xy_a + yx_a) \end{pmatrix} \\ \begin{pmatrix} \Delta Z_6(x,y) \\ \Delta Z_7(x,y) \end{pmatrix} &= -C_c \begin{pmatrix} x_c \\ y_c \end{pmatrix} \end{aligned} \quad (2)$$

Where x and y are the field position x_f and y_f define the center of the focal surface pattern, x_a and y_a define the center of the astigmatism pattern and x_c and y_c define the center of the coma pattern. C_f, C_a and C_c are the focal surface curvature, and coefficients for the radial dependence of astigmatism and coma respectively. The focal surface $C_f = 1/2R_f$ where R_f is the radius of curvature.

Setting the coma to zero in the center field centers the coma pattern, and thus in principle no additional field measurements are required to determine the center of the coma pattern. Only one field measurement of astigmatism is needed to locate the center of the astigmatism pattern. The principle axis of an astigmatism measurement determines the direction of the astigmatism pattern center and the amplitude determines the distance of the center from the measurement position. For focus two field measurements at different locations are needed to triangulate the center. In practice, multiple measurements are taken, generally a minimum of eight.

The shift in the pattern centers depends linearly on the lateral translation and tilt M2, and the tilt of M3.

C_f, C_a and C_c and expected shift of the pattern centers as a function of secondary and tertiary tilts was derived using Zemax. The coefficients are given in Table 2. These coefficients were verified empirically to by putting in large offsets in the secondary tilt (250") and the tertiary tilt (460") and recovering the corrections with errors of less than 10%.

Table 2. Collimation parameters for the Magellan telescopes. The C column specifies the parameters in equation 2. M2 shift is gives the decentering of each aberration pattern as a function of the secondary translation. M2 tilt gives the decenterings as a function of secondary tilt. M3 tilt gives the decenterings as a function of tertiary tilt.

	C	M2 shift '/μm	M2 tilt '/"	M3 tilt '/"
focus	-0.0735 μm/(')^2	0	-0.00320	0.00304
astigmatism	-0.0182 μm/(')^2	0.00037	0.00954	0.00233
coma	-0.1629 μm/(')	0.03147	0	0.00233
pointing		0.00045	-0.00285	0.00233

The Magellan telescopes have 2 Nasmyth and one folded port each. A critical part of the analysis software is calculating the coordinate transformations between the S-H camera and rotator coordinates to the coordinates of the primary, secondary, and the tertiary which is on a rotating turret to select ports.

Several systematic effects have been discovered in the two-probe data. There is residual control error measured in the central, active, probe. Our procedure effectively eliminates this systematic. In addition, there appear to be residual aberrations in the S-H probes. We fit a constant offset for the astigmatism and coma in the frame of reference of the S-H sensors. These errors can be constrained by sampling at different positions in the guider reference frame.

.

4.2 Tolerance Analysis

Repeatability measurements of the two-probe procedure indicate tilt errors of 10" to 30" in the secondary and tertiary.

A focus decenter of 0.1' produces errors that increase linearly with field radius and grow to 0.174 μm of Zernike focus at 10'. This corresponds to a uniformly filled out of focus image with a full diameter of very nearly 0.1". This should be considered a maximum error as probe distance of 10' is an extreme position in normal operation of the facility guiders. A focus decenter of 0.1' arises from an error of about 30" tilt in either the secondary or tertiary.

Astigmatism decenter of 1.0' produces errors that increase linearly with field radius and grow to 0.364 μm of Zernike astigmatism at 10'. This corresponds to a uniformly filled image with a full diameter of very nearly 0.1". Astigmatism decenter of 1.0' arises from a tilt error of 105" in the secondary or 430" of the tertiary.

The two-probe procedure thus easily collimates the telescope to an accuracy in which the field aberrations have a negligible contribution to the delivered image quality error budget.

5. TELESCOPE POINTING

The Magellan telescopes points to better than 1.5" after a new model has been implemented[3]. Pointing with this accuracy greatly increases setup efficiency. We have begun regular pointing tests to maintain this pointing accuracy. The most significant errors found in the pointing tests are those related to collimation: the elevation index error and the left-right collimation error, perpendicular to the elevation axis. The elevation index is set nightly on sky by indexing on a star of known position. It, therefore, does not impact the pointing performance. The left-right collimation can only be measured with a more extensive pointing test. We have begun a program of regular pointing tests to maintain accurate pointing.

6. PRIMARY MIRROR

In normal operation, the primary and secondary mirrors of the Magellan telescopes are actively corrected every 30 seconds by the Shack-Hartmann wavefront analysis system. The secondary mirror control system has a flexure model, but little effort had been put into characterizing or attempting to pre-correct the primary mirror. While a few iterations of the S-H system can correct the primary mirror after opening the telescope or slewing to a new field, this mode of operation reduces efficiency and can impact the ability to troubleshoot problems with the telescope optics.

MegaCam, a newly commissioned instrument on the Cassegrain port, utilizes the entire available imaging field for science and guiding CCDs, leaving is no additional space for an active optics system. Between science exposures, the optical system is corrected on-axis with a deployable Shack-Hartmann wavefront sensor. There are two guide CCDs with filters which make a longer and shorter optical path respectively than the science CCDs. These guide CCDs yield star images that are slightly on either side of focus, which are used to actively correct the telescope focus at the secondary mirror. The primary mirror aberrations must be corrected open loop during potentially long exposures.

The integrated active optics corrections were therefore monitored over an extended period to develop open loop models for control of the primary mirror. A set of wavefront data covering a period of 3 months, comprising about 50,000 measurements, was extracted from the engineering archive. Contemporaneous data on the position of the telescope, temperatures and other relevant parameters were also extracted. The data was split into tracks and the initial 10 wavefront measurements in each track were removed to exclude data where the Shack-Hartmann analysis had not settled to a steady state.

The mirror modes, other than cone mode, were found to have a consistent dependence on elevation and a model was developed to fit the data.

$$A + B(1 - \csc(el)) \tag{3}$$

where A and B linear coefficients determined for each mode and el is the telescope elevation. Significant offsets and elevation dependence were found in even the highest order measured modes.

The model was implemented by inserting a primary mirror server between the S-H analysis system and the primary cell control computer. In parallel with the S-H analysis system, a model calculator reads the elevation of the telescope every

30 seconds and sends Zernike coefficients derived from the model to the server. The primary mirror server only sends corrections to the mirror based on the coefficients received from one of the two sources. It automatically switches to sending corrections based on the model under two conditions: when no coefficients have been received from the S-H system for 75 seconds, or when the rate of elevation change of the telescope exceeds the maximum tracking speed, indicating that the telescope position on the sky has changed. The primary mirror server automatically switches back to sending corrections based on the S-H analysis as soon as an image is received from the wavefront sensor.

The corrections sent to the primary mirror based on the model are incremental; the primary mirror server only sends the difference between the current model calculation and the previous calculation to the mirror. Thus, the model and server preserve all previous corrections made to the mirror by the wavefront analysis, and only attempt to maintain the current shape of the mirror over changes in telescope elevation. In normal operation, the primary mirror model and server run in the background without input or intervention from the observer or operator, provide the open-loop control needed for MegaCam, and have reduced the time needed to correct the primary mirror after slewing to a new target from several iterations of the wavefront system to often a single iteration.

Figure 2 shows the data for a select set of modes. Table 3 shows the fit parameters for all of the modes fit. The Magellan telescopes, although identical in construction, each have a distinct response to the gravitational loads induced by tipping the telescope in elevation.

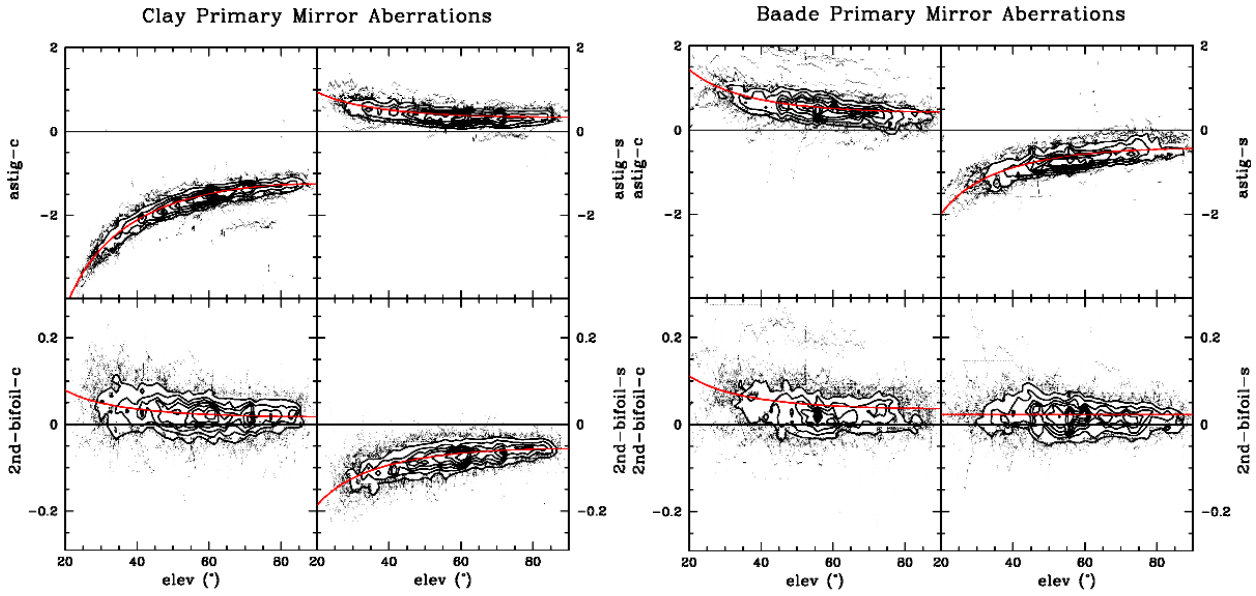

Figure 2. Examples of the dependence of primary mirror modes on elevation for the Clay and Baade telescopes. The data points show the mirror response over a period of 3 consecutive months. Contours are used to represent regions of high data density. The red lines are fits to the data using the model in equation 3.

Table 3 Fit parameters for the primary mirror mode dependence on elevation for the Clay and Baade telescopes. The RMS column gives the standard deviation of the residuals of the fit to the Zernikes.

	Clay			**Baade**		
Aberration	***A***	***B***	**RMS**	***A***	***B***	**RMS**
Astigmatism-cos	-1.249	1.550	0.16	0.432	-0.526	0.28
Astigmatism-sin	0.340	-0.315	0.14	-0.444	0.801	0.20
Trefoil-cos	0.105	0.000	0.05	-0.172	0.061	0.07
Trefoil-sin	0.000	0.000	0.08	-0.021	0.000	0.07

Quadrafoil-cos	0.004	-0.027	0.03	-0.066	0.000	0.06
Quadrafoil-sin	0.018	0.000	0.02	-0.043	0.000	0.05
2nd Bifoil-cos	0.018	-0.037	0.04	0.037	-0.039	0.04
2nd Bifoil-sin	-0.056	0.068	0.02	0.023	0.000	0.03

7. DELIVERED IMAGES

In May 2007 we began monitoring the image quality on Magellan telescope science images with ≥ 30 s exposure times. We measure the image-wide average full width at half maximum (FWHM) and shape parameters of Magellan focal plane stellar images using a program called "DIPSF" (based on DoPhot[12]) and compare them with the contemporaneous DIMM and Magellan guide camera FWHM measurements. The program has been run on all ≥ 30 s LDSS3, MagIC and IMACS images taken in 2008, as well as many from May-December 2007. We average all DIMM and guide camera measurements taken during each DIPSF exposure to give the corresponding seeing measurements for that exposure. After matching we have 876 concurrent data points from 62 nights (~10^5 stars) between May 2007 and December 2008. The DIMM FWHMs are calculated for unit airmass and nominal wavelength of 500 nm. The guide camera (λ~760nm) and DIPSF FWHM measurements are corrected to airmass 1 and to a wavelength of 0.5 μm.

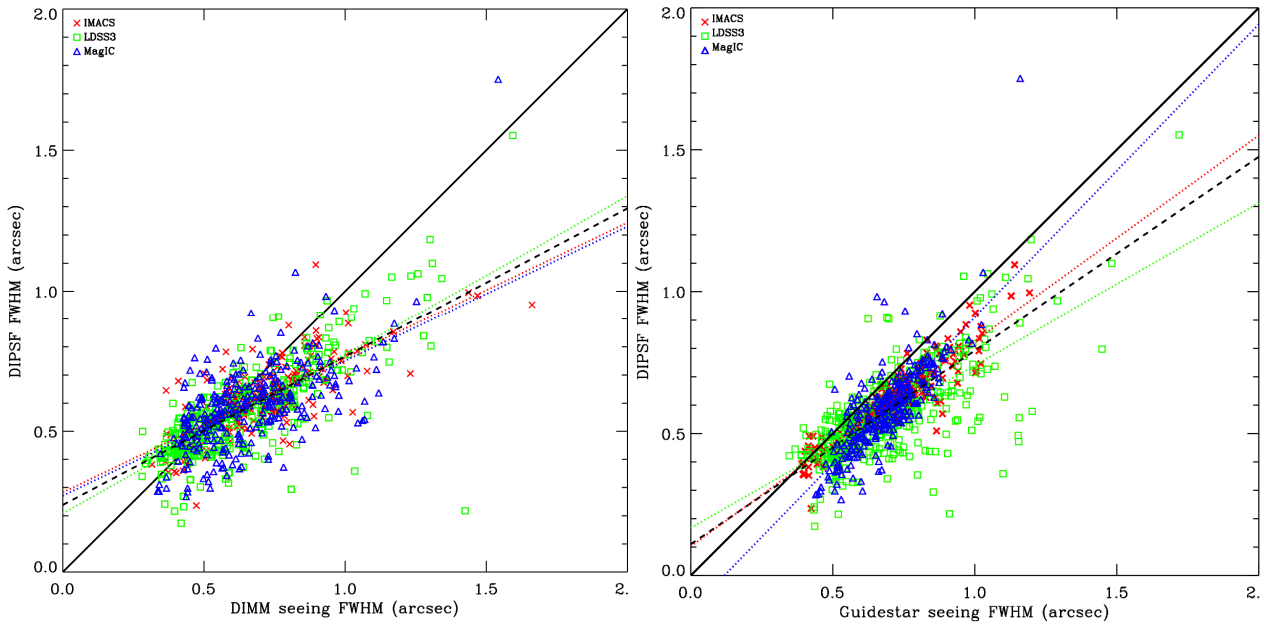

Figure 3 DIPSF seeing vs DIMM seeing (left). DIPSF seeing vs. Guidestar seeing (right)

In Fig. 2 we plot the DIPSF seeing values against simultaneous readings for the DIMM seeing (left) and guide camera seeing (right). The median DIMM seeing for our matched dataset is 0.625". The median $FWHM_{DIPSF}$ is 0.575" and for the guide cameras it is 0.688". Mean values and standard deviations are $FWHM_{DIMM}$ = 0.658" ± 0.205", $FWHM_{DIPSF}$ = 0.585" ± 0.150" and FWHMguide = 0.697" ± 0.165".

7.1 Results

The Magellan image quality is better than the DIMM seeing 69% of the time, and better than the guide camera image quality 90% of the time. In poor seeing conditions (DIMM values ≥ 1") Magellan does better than the DIMM 98% of the time. The result is qualitatively as we would expect for a large telescope: the Magellan science cameras generally return an image quality that is better than the seeing as measured by the DIMMs. At good seeing we are limited by the telescope optics, and the two readings converge, while at poor seeing, the Magellan telescopes appear to do

progressively better than would be expected from the DIMM seeing. The best linear fit to the entire dataset gives $FWHM_{DIPSF} = 0.53\ FWHM_{DIMM} + 0.24$". For the individual instruments this varies little (see Fig. 2, left panel), with LDSS3 following a slightly steeper relation than MagIC and IMACS. When comparing the DIPSF data to the guide camera FWHM there is a more marked difference between the instruments.

It is interesting to note that the IMACS DIPSF FWHM values do not get as low as those for the other instruments, in spite of having the largest number of measurements. The minimum IMACS DIPSF FWHM (excluding a single outlier at 0.24") is at 0.35". LDSS3 has a minimum FWHM at 0.22" and 17 points that are lower than the IMACS minimum (excluding a single outlier at 0.17"). MagIC has a minimum FWHM of 0.27" and 13 points that are below the IMACS minimum. This may be traceable to the averaging over a larger field of view, or inherent to the optics on the IMACS port of the telescope. The (S-H) wavefront sensors fitted to the instrument ports provide a measure of the optical aberrations present during operation of the Magellan telescopes. These predict a modal Gaussian PSF FWHM of 0.17. This is sufficient to degrade a seeing of 0.25" to 0.30". However, the S-H system on IMACS predicts a modal Gaussian PSF FWHM of 0.30", sufficient to degrade seeing of 0.25" to 0.39".

Defining $r_s = FWHM_{DIMM} - FWHM_{science}$ (such that a positive r_s implies a better science image quality than the DIMM seeing) we can investigate the improvement of Magellan image quality over DIMM seeing with various environmental factors. We find no large-scale trend of r_s with telescope pointing and conclude that there are no major directional impediments to the image quality obtained at Magellan. While there is always a weak tendency for $r_s > 0$, this becomes strongest at the highest wind speeds (and worst seeing conditions). We find that this is primarily a local effect at the DIMM[13]. Removing the high wind speed data primarily improves the DIMM distribution, with a smaller improvement seen in the DIPSF distribution. The median DIPSF image quality drops from 0.575" to 0.553", whereas the median DIMM image quality drops from 0.625" to 0.594". We find that a wavefront outer scale of turbulence L_0 H 25 m (consistent with other Chilean sites) gives a conservative estimate of the image FWHM at seeing values above 0.6". At low seeing values it seems likely that we are beginning to hit limitations imposed by the telescope optics. As discussed above, the LDSS3 and MagIC ports are slightly better than the IMACS port, but in general we would expect even the best seeing conditions (< 0.25") to return image FWHM of < 0.3"□0.4" on the instrument ports.

7.2 Conclusions

L_0 is independent of wavelength and thus the gain in image quality for a large telescope as we move redward is somewhat greater than we would expect for the strict case of Kolmogorov turbulence with infinite outer scale. If we adopt an average seeing of 0.65" and assuming $L_0 = 25$ m we would estimate that for a large telescope the ideal image quality (assuming perfect optics) at 500 nm is 0.52". In reality, we are degraded somewhat due to imperfect optics, as seen from the Shack-Hartmann system. If we extrapolate further, we estimate that the ideal image quality for a large telescope should be 0.41" at 1μm, 0.29" at 2μm, and 0.26" at 5μm.

We have presented a simple method for measuring the outer scale of turbulence that can be used at any observatory site that has a large aperture telescope used regularly for imaging, and a DIMM device for measuring the seeing. The Las Campanas Observatory site offers truly excellent seeing conditions. The effective "seeing" for the Magellan telescopes is considerably underestimated by the DIMMs. While the DIMMs give a median seeing of 0.625", the median Magellan science image FWHM is 0.575". We find the dominant cause of this difference is local to the DIMM: high wind velocities introduce local turbulence, perhaps through interaction with the clamshell dome. There is weak evidence for a directional influence on the DIMM image degradation at wind directions perpendicular to the orientation of the opening. However, removing points with wind speeds > 10 ms−1 we find that the Magellan image quality is still significantly better than the DIMM seeing. From the cumulative distributions of the DIPSF and DIMM FWHMs we estimate that the site has an average turbulence outer scale of $L_0 < 25$ m, similar to that measured at other sites.

8. SUMMARY

The Magellan telescopes deliver 0.575" FWHM image quality in science operations. We review activities to improve telescope performance and efficiency of operations.

Acknowledgements

This paper includes data gathered with the 6.5 meter Magellan Telescopes and with the GMTO DIMMs, located at Las Campanas Observatory, Chile. DF acknowledges the support of a Magellan Fellowship from Astronomy Australia Limited, and administered by the Anglo-Australian Observatory.

REFERENCES

[1] Shectman, S. A., "Optical design of the Magellan Project 6.5-meter telescope," Proc. SPIE 2199, 558 (1994)
[2] Shectman, S. A., "Magellan project," Proc. SPIE 4004, 47 (2000).
[3] Shectman, S. A. and Johns, M., "The Magellan Telescopes," Proc. SPIE 4837, 910 (2003).
[4] Schechter, P. L., Burley, G. S., Hull, C.L., Johns, M., Martin, H. M., Schaller, S., Shectman, S. A. and West, S. C., "Active optics on the Baade 6.5-m (Magellan I) Telescope," Proc. SPIE 4837, 619 (2003).
[5] Martin, H. M., Callahan, S. P., Cuerden, B., Davison, W. B.; Derigne, S. T., Dettmann, L. R., Parodi, G., Trebisky, T. J., West, S. C. and Williams, J. T., "Active supports and force optimization for the MMT primary mirror," Proc SPIE 3352, 412 (1998).
[6] Martin, H. M., Allen, R. G. Cuerden, B., DeRigne, S. T., Dettmann, L. R., Ketelsen, D. A., Miller, S M., Parodi, G. and Warner, S., "Primary mirror system for the first Magellan telescope," Proc. SPIE 4003, 2 (2000).
[7] Martin, H. M., Allen, R. G.; Burge, J. H.; Dettmann, L. R.; Ketelsen, D. A.; Miller, S. M., III; Sasian, J. M., "Fabrication of mirrors for the Magellan Telescopes and the Large Binocular Telescope," Proc SPIE 4837, 609, (2003).
[8] Shack, R. V. and Thompson, K., "Influence of alignment errors of a telescope system on its aberration field," Proc. SPIE 251, 146 (1980).
[9] Mcleod , B. A. "Collimation of Fast Wide-Field Telescopes," PASP 108, 217 (1996).
[10] Gitton, Ph., Noethe, L. "Tuning of the NTT Alignment," The Messanger 192, 15-18 (1998).
[11] Floyd, D. J. E., Thomas-Osip, J. and Prieto, G., "Seeing, Wind and Outer Scale Effects on Image Quality at the Magellan Telescopes," PASP 122, 731 (2010).
[12] Schechter, P. L., Mateo, M., and Saha, A., "DOPHOT, a CCD photometry program: Description and tests," PASP 105, 1342 (1993).
[13] Sarazin, M., "Instrumentation for site evaluation in Northern Chile," Proc. SPIE 628, 138 (1986).